

Surface and zeta potentials of charged permeable nanocoatings

Elena F. Silkina,¹ Naren Bag,² and Olga I. Vinogradova^{1,2,*}

¹*Frumkin Institute of Physical Chemistry and Electrochemistry,*

Russian Academy of Sciences, 31 Leninsky Prospect, 119071 Moscow, Russia

²*DWI - Leibniz Institute for Interactive Materials, Forckenbeckstr. 50, 52056 Aachen, Germany*

(Dated: January 5, 2022)

An electrokinetic (zeta) potential of charged permeable porous films on solid supports generally exceeds their surface potential, which often builds up to a quite high value itself. Recent work provided a quantitative understanding of zeta potentials of thick, compared to the extension of an inner electrostatic diffuse layer, porous films. Here, we consider porous coatings of a thickness comparable or smaller than that of the inner diffuse layer. Our theory, which is valid even when electrostatic potentials become quite high and accounts for a finite hydrodynamic permeability of the porous materials, provides a framework for interpreting the difference between values of surface and zeta potentials in various situations. Analytic approximations for the zeta potential in the experimentally relevant limits provide a simple explanation of transitions between different regimes of electro-osmotic flows, and also suggest strategies for its tuning in microfluidic applications.

Keywords: Electroosmosis; porous coatings; zeta-potential; surface potential

I. INTRODUCTION

A century ago von Smoluchowski [1] proposed an equation to describe a plug electro-osmotic flow in a bulk electrolyte that emerges when an electric field E is applied at tangent to a charged solid surface. He related the velocity in the bulk V_∞ to the electrokinetic (zeta) potential of the surface Z . For canonical solid surfaces with *no-slip* hydrodynamic boundary condition, simple arguments lead to $Z = \Psi_s$, where Ψ_s is the surface (electrostatic) potential. However, the problem is not that simple and has been revisited in last decades. For example, even ideal solids, which are smooth, impermeable, and chemically homogeneous, can modify the hydrodynamic boundary conditions when poorly wetted [2], and the emerging hydrophobic slippage can augment Z compared to the surface potential [3–6]. Furthermore, most solids are not ideal but rough and heterogeneous. This can further change, and quite dramatically, the boundary conditions [7] leading to a very rich electro-osmotic behavior and, in some situations (e.g. superhydrophobic surfaces), providing a huge flow enhancement compared to predicted by the Smoluchowski model [8–10].

The defects or pores of the wettable solids also modify the hydrodynamic boundary condition [11]. Besides, the local electro-neutrality is broken not only in the outer diffuse layer as it occurs for impenetrable surfaces [12, 13], but also in the inner one [14]. Moreover, even when the porous coating is electrostatically thick, i.e. includes a globally electro-neutral region, only mobile adsorbed ions can react to an applied electric field [15]. Consequently, the electric volume force that drives the electro-osmotic flow in the electro-neutral bulk electrolyte is now generated inside the porous material too. This suggests that one can significantly impact the electro-kinetic

response of the whole macroscopic system, i.e. of the bulk electrolyte, just by using various permeable nanometric coatings at the solid support, such as polyelectrolyte networks, multilayers, and brushes [16–20], or ultrathin porous membrane films [21–23].

The emerging flow is strongly coupled to the electrostatic potential profile that sets up self-consistently, so the latter becomes a very important consideration in electroosmosis involving porous surfaces. Electrostatic potentials, Ψ_s and Ψ_0 at the solid support, have been studied theoretically over several decades. In most of these studies weakly charged surfaces or thick compared to their inner screening length porous films have been considered [14, 24–26]. Very recently Silkina *et al.* [27] reported a closed-form analytic solution for Ψ_0 , obtained without a small potential assumption, which is valid for porous films of any thickness. These authors also proposed a general relationship between Ψ_s and Ψ_0 , but made no attempts to derive simple asymptotic approximations for surface potentials that could be handled easily.

The connection between the electro-osmotic velocity and electrostatic potentials have been reported by several groups [24–26, 28–30], and these models are frequently invoked in the interpretation of the electrokinetic data [31]. However, despite its fundamental and practical significance, the zeta-potential of porous surfaces has received so far little attention, and its relation to Ψ_s has remained obscure until recently. Some authors concluded that the zeta-potential ‘loses its significance’ [25], ‘irrelevant as a concept’ [32] or ‘is undefined and thus nonapplicable’ [28], while others reported that Z typically exceeds Ψ_s [33, 34], but did not attempt to relate their results to the inner flow and emerging liquid velocity at the porous surface. This was taken up only recently in the paper by Vinogradova *et al.* [15], who carried out calculations of the zeta potential for thick coatings of both an arbitrary volume charge density and

* Corresponding author: oivinograd@yahoo.com

a finite hydrodynamic permeability. These authors predicted that Z is generally augmented compared to the surface electrostatic potential, thanks to a liquid *slip* at their surface emerging due to an electro-osmotic flow in the enriched by counter-ions porous films. However, this work cannot be trivially extended to the case of non-thick films, where inner electrostatic potential profiles are always, and often essentially, inhomogeneous. These profiles can be calculated assuming that electrostatic potentials are low [14], but such an assumption becomes unrealistic in many situations. Recently, Silkina *et al.* [27] derived rigorous upper and lower bounds on Z of non-thick films, by lifting an assumption of low electrostatic potential. However, we are unaware of any prior work that investigated the connection of the zeta potential of non-thick films with their finite hydrodynamic permeability.

In this paper, we provide analytical solutions to electro-osmotic flows in and outside uniformly charged non-thick porous coatings, with the focus on their zeta potential and its relation to the surface potential. Ionic solutions are described using the non-linear mean-field Poisson-Boltzmann theory. For simplicity, here we treat only the symmetric monovalent electrolyte, but it is rather straightforward to extend our results to multivalent ionic systems. As any approximation, the Poisson-Boltzmann formalism has its limits of validity, but it always describes very accurately the ionic distributions for monovalent ions in the typical concentration range from 10^{-6} to 10^{-1} mol/L [35]. Since in this concentration range λ_D decreases from ca. 300 down to 1 nm [36], the non-thick films we discuss are of nanometric thickness. We show that the nanofluidic transport inside such films depends on several nanometric length scales, leading to a rich macroscopic response of the whole system. In particular, we demonstrate that the zeta-potential of non-thick coatings becomes a property, defined by the relative values of their thickness, the Brinkman and Debye screening lengths, and of another electrostatic length ℓ , which depends on the volume charge density, but not on the salt concentration.

In Sec. II we give basic principles, brief summary of known relationships, and formulate the problem. Solutions to electro-osmotic velocities and zeta-potentials are derived in Sec. III. We illustrate the theory and validate it numerically in Sec. IV. Implications for the use of non-thick porous films to enhance electro-osmotic flows at different salt concentration are discussed in Sec. V, followed by concluding remarks in Sec. VI

II. MODEL, GOVERNING EQUATIONS, AND SUMMARY OF KNOWN RELATIONSHIPS

The system geometry is shown in Fig. 1. The properties of the sketched heterogeneous supported film are, of course, related to its internal structure and can be evaluated in specific situations, but here we do not try to solve

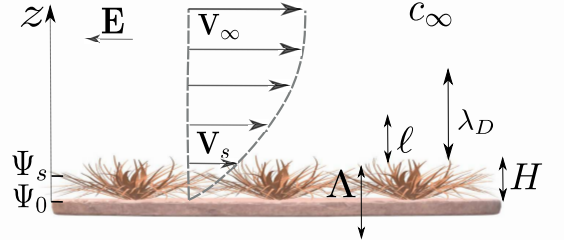


FIG. 1. Permeable non-thick coating of thickness H and positive volume charge density ρ in contact with a bulk electrolyte solution of concentration c_∞ . The wall, Ψ_0 , and surface, Ψ_s , electrostatic potentials are build up self-consistently and defined, besides H , by two lengths, $\lambda_D \propto c_\infty^{-1/2}$ and $\ell \propto \rho^{-1/2}$. The application of a tangential electric field, E , leads to an electro-osmotic flow of solvent that depends on the Brinkman screening length Λ . The velocity at the surface of a porous film is V_s , and that in the bulk is V_∞ .

the problem at the scale of the individual pores. Instead, motivated by the theory of heterogeneous media [37, 38], we replace such a real coating by an imaginary homogeneous one, which ‘macroscopically’ behaves in the same way and possess effective properties, such as a volume charge density or a hydrodynamic permeability. Thus, we consider a homogeneous permeable film of a thickness H , which sets a length scale for our problem, of a volume charge density ρ , taken positive without loss of generality.

The film is in contact with a semi-infinite 1:1 electrolyte of bulk ionic concentration c_∞ , permittivity ϵ , and dynamic viscosity η . Ions obey Boltzmann distribution, $c_\pm(z) = c_\infty \exp(\mp \psi(z))$, where $\psi(z) = e\Psi(z)/(k_B T)$ is the dimensionless electrostatic potential, e is the elementary positive charge, k_B is the Boltzmann constant, T is a temperature, and the upper (lower) sign corresponds to the cations (anions). In the bulk, i.e. far away from the coating ($z \rightarrow \infty$), an electrolyte solution is electro-neutral, $c_\pm(z) = c_\infty$, and $\psi(\infty) \rightarrow 0$. The inverse Debye screening length of an electrolyte solution, $\kappa \equiv \lambda_D^{-1}$, is defined as usually, $\kappa^2 = 8\pi\ell_B c_\infty$, with the Bjerrum length $\ell_B = \frac{e^2}{\epsilon k_B T}$. The Debye length defines a new (electrostatic) length scale and is the measure of the thickness of the outer diffuse layer, where the local electro-neutrality is broken. We emphasize that it is independent on the film charge.

The system subjects to a weak tangential electric field E , so that in steady state $\psi(z)$ is independent of the fluid flow. For our geometry the concentration gradients at every location are perpendicular to the direction of the flow, it is therefore legitimate to neglect advection. Consequently, the dimensionless velocity of an electro-osmotic flow, $v(z) = \frac{4\pi\ell_B\eta}{eE}V(z)$, satisfies the generalized Stokes equation [39]

$$v''_{i,o} - \mathcal{K}^2 v_{i,o} \Theta(H - z) = \psi''_{i,o} + \kappa^2 \rho \Theta(H - z), \quad (1)$$

where ' denotes d/dz , with the index $\{i, o\}$ standing for "in" ($z \leq H$) and "out" ($z \geq H$), $\Theta(z)$ is the Heaviside step function, $\mathcal{K} = \Lambda^{-1}$ is the inverse Brinkman length, and $\rho = \frac{q}{2ec_\infty}$. For small volume charge and/or high electrolyte concentration ρ is small and below we refer such coatings to as weakly charged. For large volume charge and/or dilute electrolyte solutions ρ is large and we term these films strongly charged. The Brinkman length can theoretically vary from 0 to ∞ . In the latter (idealized) case an additional dissipation in the porous film is neglected. If so, the hydrodynamic permeability of the porous film reaches its highest possible limit and $\propto H^2$ [15]. In the former case of vanishing Λ the additional dissipation inside the coating is so high that the porous film permeability ($\propto \Lambda^2$) tends to zero, i.e. the inner flow is fully suppressed. In reality, however Λ is finite and defined by the parameters of the porous film, such, for example, as volume fraction of the solid, size of the pores, and their geometry.

At the wall we apply a classical no-slip condition, $v_0 = v_i(0) = 0$, and at the surface the condition of continuity of velocity, $v_i(H) = v_o(H)$, and shear rate, $v'_i(H) = v'_o(H)$, is imposed. Far from the surface, the solution of Eq.(1) should satisfy $v'_o \rightarrow 0$ at $z \rightarrow \infty$ to provide a plug flow. The velocity v_∞ at $z \rightarrow \infty$ is constant and equal to $-\zeta$.

The dimensionless zeta-potential, $\zeta = eZ/(k_B T)$ is given by [15, 27]

$$\zeta = \psi_s - v_s, \quad (2)$$

where $\psi_s = e\Psi_s/(k_B T)$ and $v_s = v(H)$. Note that $-v_s$ represents the velocity jump inside the porous film. Any situation where the value of the tangential component of velocity appears to be different from that of the solid surface is normally termed slip [7]. Therefore, $-v_s$ represents the (positive definite) slip velocity of liquid at the film surface, $z = H$. As a side note, since the film with an outer diffuse layer is much thinner than any of the macroscopic dimensions, the bulk liquid also appears to slip, but with the velocity $-v_\infty$. By this reason in colloid science $-v_\infty$ is often termed an apparent electro-osmotic slip velocity. [40]. To distinguish between real and apparent slip, and recalling that $-v_\infty = \zeta$, below we will refer this (dimensionless) apparent slip to as ζ .

Silkina *et al.* [27] carried out calculations in the limit of zero and infinite $\mathcal{K}H$ and concluded that for films of an arbitrary thickness at $\mathcal{K}H \rightarrow 0$

$$-v_s \simeq \Delta\psi + \frac{\rho(\kappa H)^2}{2}, \quad \zeta \simeq \psi_0 + \frac{\rho(\kappa H)^2}{2}, \quad (3)$$

and

$$-v_s \simeq 0, \quad \zeta \simeq \psi_s \quad (4)$$

when $\mathcal{K}H \rightarrow \infty$. Here $\psi_0 = e\Psi_0/(k_B T) = \psi(0)$ is the wall potential, $\psi_s = \psi(H)$ is the surface potential, and $\Delta\psi = \psi_0 - \psi_s$ is the drop of the electrostatic potential in the coating.

TABLE I. Various limits of electrostatic "thickness" for a porous film of a (geometric) thickness H .

Electrostatic thickness	Weakly charged films ($\rho \ll 1$)	Highly charged films ($\rho \gg 1$)
thick	$\kappa H \gg 1$	$\kappa H \sqrt{\rho} \gg 1$
non-thick	$\kappa H \not\gg 1$	$\kappa H \sqrt{\rho} \not\gg 1$
thin	$\kappa H \ll 1$	$\kappa H \sqrt{\rho} \ll 1$

Eqs.(3) and (4) represent rigorous upper and lower bounds that constrain the attainable values of slip velocity and zeta-potential. In many regimes, however, these bounds are not close enough to obviate the need for calculations flows over porous surfaces of a finite $\mathcal{K}H$.

It follows from Eq.(1) that to calculate electro-osmotic velocity we have to find the distribution of electrostatic potentials that satisfy the nonlinear Poisson-Boltzmann equation

$$\psi''_{i,o} = \kappa^2 (\sinh \psi_{i,o} - \rho \Theta(H - z)), \quad (5)$$

and to obtain simple expressions for ψ_0 , ψ_s , and $\Delta\psi$. We assume that the wall is uncharged, $\psi'_i(0) = 0$, and set $\psi_i(H) = \psi_o(H)$ and $\psi'_i(H) = \psi'_o(H)$ at the surface of the coating.

The solution of Eq.(5) satisfying $\psi_o \rightarrow 0$ and $\psi'_o \rightarrow 0$ at $z \rightarrow \infty$ is the same as for an impenetrable wall of the same ψ_s [35]

$$\psi_o(z) = 4 \operatorname{artanh} \left[\gamma e^{-\kappa(z-H)} \right], \quad (6)$$

where $\gamma = \tanh \frac{\psi_s}{4}$.

Ions of an outer electrolyte can permeate inside the porous film, giving rise to their homogeneous equilibrium distribution in the system, with the enrichment of anions in the film. When $\kappa H(1 + \rho^2)^{1/4} \gg 1$ the film becomes thick compared to the inner diffuse layer, with an extended 'bulk' electro-neutral region (where intrinsic coating charge is completely screened by absorbed electrolyte ions, is formed). The potential in this region is usually referred to as the Donnan potential, ψ_D . Note that Eq.(5) immediately suggests that $\psi_D = \operatorname{arsinh}(\rho)$ since in the electro-neutral area ψ'_i vanishes. A systematic treatment of the influence of the Brinkman length on the zeta-potential of thick films was contained in a paper published by Vinogradova *et al.* [15]. Here we will focus on the case of films of

$$\kappa H(1 + \rho^2)^{1/4} \not\gg 1 \quad (7)$$

that can be termed non-thick. For weakly charged films of $\rho \ll 1$ this implies that $\kappa H = O(1)$ or smaller. The

more interesting strongly charged coatings of $\rho \gg 1$ can be considered as non-thick when $\kappa H \sqrt{\rho} \gg 1$ and are thin when $\kappa H \sqrt{\rho} \ll 1$. For convenience in Table I we give a summary of criteria defining different limits for an electrostatic thickness.

Non-thick films do not contain an electro-neutral portion, where the intrinsic volume charge is fully screened by absorbed ions. Consequently, their ψ_0 given by [27]

$$\psi_0 \simeq \ln \left[\frac{2 + (\rho \kappa H)^2 + \rho \kappa H \sqrt{4 + (\kappa H)^2(1 + \rho^2)}}{2 + \rho(\kappa H)^2} \right]. \quad (8)$$

is smaller than the Donnan potential.

The surface potential, ψ_s , and the potential drop in the film, $\Delta\psi = \psi_0 - \psi_s$, are related to ψ_0 as [6, 27]

$$\psi_s \equiv \psi_0 - \frac{\cosh \psi_0 - 1}{\rho}, \quad \Delta\psi = \frac{\cosh \psi_0 - 1}{\rho}. \quad (9)$$

The inner ψ -profile of a non-thick film is given by [27]

$$\psi_i(z) \simeq \psi_0 - \frac{\rho}{2} (\kappa z)^2 [1 - \mathcal{F}], \quad (10)$$

where

$$\mathcal{F} = \frac{\sinh \psi_0}{\rho} \quad (11)$$

represents the fraction of the screened film intrinsic charge at $z = 0$.

The surface potential is then

$$\psi_s \simeq \psi_0 - \frac{\rho}{2} (\kappa H)^2 [1 - \mathcal{F}]. \quad (12)$$

III. ELECTROSTATIC POTENTIALS VS. ZETA-POTENTIAL

The expression for an outer velocity can be written as [15, 27]

$$v_o(z) = v_s + \psi_o(z) - \psi_s, \quad (13)$$

where ψ_o is given by Eq.(6) and ψ_s obeys Eq.(12). Therefore, in order to obtain a detailed information concerning zeta-potential a calculation of v_s arising due to the inner flow is required.

We have calculated the inner velocity profile by solving Eq.(1) with ψ_i satisfying Eq.(10) and prescribed boundary conditions, and obtained that v_i is given by

$$v_i = \left(\rho \left(\frac{\kappa}{\mathcal{K}} \right)^2 - \frac{2\Delta\psi}{(\mathcal{K}H)^2} \right) (e^{-\mathcal{K}z} - 1) + \frac{\sinh \mathcal{K}z}{\cosh \mathcal{K}H} \left[\left(\rho \left(\frac{\kappa}{\mathcal{K}} \right)^2 - \frac{2\Delta\psi}{(\mathcal{K}H)^2} \right) e^{-\mathcal{K}H} - \frac{2\Delta\psi}{\mathcal{K}H} \right]. \quad (14)$$

so that at the surface

$$v_s = \left[\rho (\kappa H)^2 - 2\Delta\psi \right] \frac{(1 + \tanh \mathcal{K}H)e^{-\mathcal{K}H} - 1}{(\mathcal{K}H)^2} - 2\Delta\psi \frac{\tanh \mathcal{K}H}{\mathcal{K}H}, \quad (15)$$

Eq.(15) can be used for any values of ρ and $\mathcal{K}H$, and in the limits of $\mathcal{K}H \rightarrow 0$ and ∞ reduces to Eqs.(3) and (4).

When $\mathcal{K}H$ is small, Eq.(15) can be expanded about $\mathcal{K}H = 0$, and to second order we obtain

$$-v_s \simeq \Delta\psi \left(1 - \frac{(\mathcal{K}H)^2}{4} \right) + \frac{\rho(\kappa H)^2}{2} \left(1 - \frac{5(\mathcal{K}H)^2}{12} \right) \quad (16)$$

The first term in Eq.(16) is associated with the reduction of the potential, $\Delta\psi$, in the porous film, but also depends on $\mathcal{K}H$. The second term is associated with a body force $\rho\kappa^2$ that drives the inner flow. Both terms reduce with $\mathcal{K}H$ leading to deviations from the upper value of $-v_s$ defined by Eq.(3). Using then (2) we conclude that the ζ -potential can be approximated by

$$\zeta \simeq \psi_0 - \Delta\psi \frac{(\mathcal{K}H)^2}{4} + \frac{\rho(\kappa H)^2}{2} \left(1 - \frac{5(\mathcal{K}H)^2}{12} \right) \quad (17)$$

Expanding v_s in Eq.(15) at large $\mathcal{K}H$ we find

$$-v_s \simeq \frac{2\Delta\psi}{\mathcal{K}H} + \rho \left(\frac{\kappa}{\mathcal{K}} \right)^2 \quad (18)$$

Eq.(18) indicates that v_s is a superposition of a flow that is linear in $\Delta\psi$ and of a plug flow, $\rho \left(\frac{\kappa}{\mathcal{K}} \right)^2$. Then it follows from Eq.(2) that

$$\zeta \simeq \psi_s + \frac{2\Delta\psi}{\mathcal{K}H} + \rho \left(\frac{\kappa}{\mathcal{K}} \right)^2 \quad (19)$$

Thus, our treatment clarifies that at a given $\mathcal{K}H$, a slip velocity $-v_s$ (and a consequent ζ) can be enhanced by generating larger $\Delta\psi$ and/or when $\rho(\kappa H)^2$ is large. When both are small, $-v_s \simeq 0$ and $\zeta \simeq \psi_s$.

The value of ψ_0 can be generally calculated from Eq.(8), which then allows to find ψ_s and $\Delta\psi$ from Eq.(9). Using standard manipulations we derive

$$\Delta\psi \simeq \frac{\rho(\kappa H)^2}{2 + \rho(\kappa H)^2} \left(1 + \frac{(\kappa H)^2(1 - \rho) - \kappa H \sqrt{4 + (\kappa H)^2(1 + \rho^2)}}{2 + (\rho\kappa H)^2 + \rho\kappa H \sqrt{4 + (\kappa H)^2(1 + \rho^2)}} \right) \quad (20)$$

and

$$\mathcal{F} \simeq \frac{2 + (\rho\kappa H)^2}{2\rho + (\rho\kappa H)^2} - \frac{2}{\rho(2 + (\rho\kappa H)^2 + \rho\kappa H \sqrt{4 + (\kappa H)^2(1 + \rho^2)})} \quad (21)$$

These two last equations are expected to be very accurate, but are quite cumbersome. Fortunately, in some limits they can be dramatically simplified leading to very simple analytic solutions for ζ . We discuss now separately two limits, depending on how strong the dimensionless volume charge density is.

A. Weakly charged coatings ($\rho \ll 1$)

At small ρ one can expand ψ_0 given by Eq.(8) into a series about $\rho = 0$, and we conclude that a sensible approximation for ψ_0 should be

$$\psi_0 \simeq \rho\kappa H \frac{\sqrt{4 + (\kappa H)^2} - \kappa H}{2}. \quad (22)$$

Note that ψ_0 is linear in ρ , but is a non-linear function of κH since to derive Eq.(22) we do not make an additional assumption that $\kappa H \ll 1$. Consequently, this and following equations of this subsection should be valid even when $\kappa H = O(1)$.

Expanding Eq.(9) at small ψ_0 and substituting Eq.(22) we obtain

$$\Delta\psi \simeq \frac{\psi_0^2}{2\rho} \simeq \frac{\rho(\kappa H)^2(\sqrt{4 + (\kappa H)^2} - \kappa H)^2}{8}, \quad (23)$$

which together with (22) leads to

$$\psi_s \simeq \frac{\rho\kappa H}{4} \left(\sqrt{4 + (\kappa H)^2}(2 + (\kappa H)^2) - \kappa H(4 + (\kappa H)^2) \right) \quad (24)$$

Note that imposing the condition of small κH one can easily recover the known result of the linearized Poisson-Boltzmann theory (see Appendix A)

$$\psi_0 \simeq \rho\kappa H \left(1 - \frac{\kappa H}{2} \right), \quad \psi_s \simeq \rho\kappa H (1 - \kappa H), \quad (25)$$

which suggests that the ψ -profile is almost constant throughout a weakly charged thin film.

Expanding Eq.(11) at small ψ_0 and using Eq.(22) we get

$$\mathcal{F} \simeq \frac{\psi_0}{\rho} = \frac{\kappa H(\sqrt{4 + (\kappa H)^2} - \kappa H)}{2} + O(\rho^2) \quad (26)$$

We remark that in this low ρ regime to leading order \mathcal{F} does not depend on ρ , and is finite even if $\rho \rightarrow 0$, where $\psi_0 \simeq 0$. At first sight this is somewhat surprising, but we recall that our dimensionless charge density is introduced by dividing the real one by the salt concentration, so that a nearly vanishing ρ simply implies that the (non-thick) film is enriched by counter-ions that partly screen its intrinsic charge.

It is clear that ψ_0 , ψ_s , and $\Delta\psi$ are small, so is v_s given by Eq.(16). Consequently, ζ is also generally small and we do not discuss it here in detail. However, it would be worthwhile to mention that an upper bound on ζ in this case is

$$\zeta \simeq \rho\kappa H \frac{\sqrt{4 + (\kappa H)^2}}{2}, \quad (27)$$

which together with (24) gives $\zeta/\psi_s \simeq 2 + \kappa H \left(1 - \frac{(\kappa H)^2}{8} \right)$. Thus, the electro-osmotic flow in the bulk can potentially be enhanced in more than two times compared to the Smoluchowski case.

B. Strongly charged coatings ($\rho \gg 1$)

For strongly charged coatings Eq.(8) reduces to [27]

$$\psi_0 \simeq 2 \operatorname{arsinh} \left(\frac{\rho\kappa H}{2} \right) - \ln \left(1 + \frac{\rho(\kappa H)^2}{2} \right). \quad (28)$$

Straightforward calculations show that Eqs.(20) and (21) can be transformed to

$$\Delta\psi \simeq \frac{\rho(\kappa H)^2}{2 + \rho(\kappa H)^2}, \quad (29)$$

$$\mathcal{F} \simeq \frac{2 + (\rho\kappa H)^2}{2\rho + (\rho\kappa H)^2} \simeq \Delta\psi + \frac{2}{\rho(2 + \rho(\kappa H)^2)}, \quad (30)$$

indicating that $\Delta\psi \simeq \mathcal{F}$ when ρ is large.

Two limits can now be distinguished depending on the value of $\rho(\kappa H)^2$.

1. The limit of $\rho(\kappa H)^2 \ll 1$

We recall that since ρ is large, the film becomes thin when $\kappa H \sqrt{\rho} \ll 1$ (see Table I). Therefore, such a situation is possible only for films that are truly or relatively thin (below we refer the latter to as *quasi-thin*). We further remark that in this limit the first term in Eq.(28) dominates, so that it can be further simplified to give

$$\psi_0 \simeq 2 \operatorname{arsinh}\left(\frac{\rho \kappa H}{2}\right) - \frac{\rho(\kappa H)^2}{2} \quad (31)$$

In turn, Eq.(29) reduces to

$$\Delta\psi \simeq \frac{\rho(\kappa H)^2}{2}, \quad (32)$$

leading to

$$\psi_s \simeq 2 \operatorname{arsinh}\left(\frac{\rho \kappa H}{2}\right) - \rho(\kappa H)^2 \quad (33)$$

When $\rho \kappa H$ is small, Eqs.(31) and (33) reduce to Eqs.(25), which implies that they can also be employed when ρ is small, provided κH is not large.

From Eq.(17) we then find that for small $\mathcal{K}H$ the zeta-potential can be approximated as

$$\zeta \simeq 2 \operatorname{arsinh}\left(\frac{\rho \kappa H}{2}\right) - \frac{\rho(\kappa H)^2(\mathcal{K}H)^2}{3}, \quad (34)$$

which leads to

$$\zeta \simeq 2 \operatorname{arsinh}\left(\frac{\rho \kappa H}{2}\right) \quad (35)$$

when $\mathcal{K}H \rightarrow 0$. However, using (33) we obtain $\zeta - \psi_s \leq \rho(\kappa H)^2$, which is small in this limit. Therefore, our asymptotic arguments suggest that even in the case of extremely large hydrodynamic permeability of the porous layer, the difference between ζ and ψ_s cannot be significant. Thus a knowledge of ψ_s should be sufficient to provide a realistic evaluation of ζ (and vice versa). Nevertheless, for completeness we mention that at large $\mathcal{K}H$ from (19) one can obtain

$$\zeta \simeq 2 \operatorname{arsinh}\left(\frac{\rho \kappa H}{2}\right) + \rho \left(\frac{\kappa}{\mathcal{K}}\right)^2 (1 + \mathcal{K}H - (\mathcal{K}H)^2), \quad (36)$$

which tends to ψ_s given by Eq.(33) when $\mathcal{K}H \rightarrow \infty$.

2. The limit of $\rho(\kappa H)^2 \gg 1$

This limit is close to, but weaker of, the condition for a thick film $\kappa H \sqrt{\rho} \gg 1$ (see Table I). So, we can term these films *quasi-thick*.

For large $\rho(\kappa H)^2$, Eqs.(28) and (29) can be further simplified to

$$\psi_0 \simeq \ln(2\rho) - \frac{2}{\rho(\kappa H)^2}, \quad \Delta\psi \simeq 1 - \frac{2}{\rho(\kappa H)^2} \quad (37)$$

which gives the same ψ_s as for thick films [15, 41]

$$\psi_s \simeq \ln(2\rho) - 1 \quad (38)$$

Substituting (37) into (17) in the limit $\mathcal{K}H \ll 1$ we obtain

$$\zeta \simeq \ln(2\rho) + \frac{\rho(\kappa H)^2}{2} \left(1 - \frac{5(\mathcal{K}H)^2}{12}\right), \quad (39)$$

which suggests that for quasi-thick films ζ can become very large and significantly exceeds ψ_s .

Substitution of Eqs.(37) and (38) into (19) for $\mathcal{K}H \gg 1$ leads to

$$\zeta \simeq \ln(2\rho) - 1 + \rho \left(\frac{\kappa}{\mathcal{K}}\right)^2 + \frac{2}{\mathcal{K}H} \quad (40)$$

IV. NUMERICAL RESULTS AND DISCUSSION

It is of considerable interest to compare exact numerical data with our analytical theory and to determine the regimes of validity of asymptotic results. Here we first present results of numerical solutions of Eq.(5) with prescribed boundary conditions, using the collocation method [42]. We then solve numerically the system of Eqs.(1) and (5). The exact numerical solutions will be presented together with calculations from the asymptotic approximations derived in Sec.III.

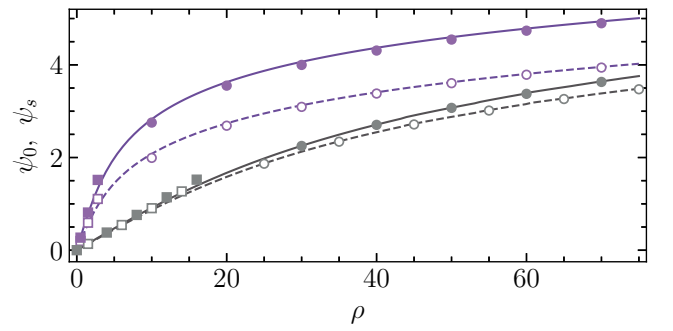


FIG. 2. Potentials at wall (solid lines) and surface (dashed) as a function of ρ computed for fixed $\kappa H = 0.8$ (upper set of curves) and $\kappa H = 0.1$ (lower curves). Filled and open squares illustrate calculations from Eqs.(22) and (24). Filled and open circles are obtained using Eqs.(37) and (38). Filled and open triangles correspond to Eqs.(31) and (33). Dash-dotted lines show ψ_0 from Eq.(A3).

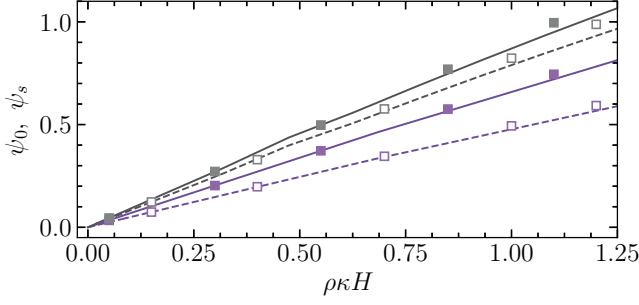


FIG. 3. The data sets for ψ_0 and ψ_s obtained at smaller values of ρ reproduced from Fig. 2 and plotted as a function of $\rho\kappa H$. The upper set of curves and symbols shows $\kappa H = 0.1$, the lower one corresponds to $\kappa H = 0.8$.

In Fig. 2 we plot ψ_0 and ψ_s , computed using $\kappa H = 0.8$ and 0.1 , as a function of ρ . It is well seen that for a thinner film $\psi_0 \approx \psi_s$ up to $\rho\kappa H \approx 3$. On increasing ρ further $\Delta\psi$ increases slowly. For a thicker film of $\kappa H = 0.8$ the potential drop in the film is always finite and $\Delta\psi$ grows much faster as ρ is increased. The theoretical curves calculated from Eqs.(22) and (24) are also included in Fig. 2. The fits are quite good for $\rho \leq 2$, but at larger ρ there is some discrepancy, especially for $\kappa H = 0.8$, and the theoretical potentials predicted by low ρ approximations become higher than computed. Note, however, that for $\kappa H = 0.1$ the discrepancy between a linear fit and numerical calculations is negligibly small when $\rho \leq 2$. To examine its significance more closely, the initial portions of the ψ -profiles from Fig. 2 are reproduced in Fig. 3, but now plotted as a function of $\rho\kappa H$. An overall conclusion from this plot is that the approximations derived in Sec.III A are very accurate when $\rho\kappa H \leq 1$. We now return to Fig. 2 and focus on the large ρ portions of the curves. As reported by Silkina *et al.* [27], Eq.(8) fits very accurately the numerical data for ψ_0 at any ρ , so does more elegant (28), except for $\rho \leq 1$, where some very small discrepancy is observed. Calculations with our parameters fully confirm this conclusion, so that we do not show these data. Instead, we include ψ_0 calculated from Eqs.(31) and (37) that correspond to small and large $\rho(\kappa H)^2$. It is well seen that for $\rho \geq 10$ the agreement with numerical data is excellent in both cases. Also included is ψ_s from (38) and (33), and we see that these asymptotic approximations coincide with the numerical data.

Fig. 4 shows the electrostatic potential drop, $\Delta\psi$, inside the film computed for $\kappa H = 0.2$ and 0.8 as a function of ρ . The degree of screened intrinsic charge at the wall, \mathcal{F} , calculated numerically for the same values of κH is also plotted. It is seen that $\Delta\psi$ first increases linearly with ρ and, when ρ is getting sufficiently large, slowly approaches to unity for a film of $\kappa H = 0.8$. However, in a chosen interval of ρ the potential drop of a thinner film of $\kappa H = 0.2$ still continues to grow, although weakly and nonlinearly. It can be seen that the linear portions of the

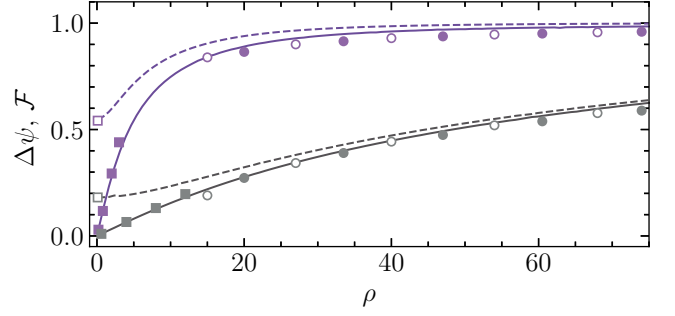


FIG. 4. $\Delta\psi$ (solid curves) and \mathcal{F} (dashed curves) vs ρ computed using $\kappa H = 0.8$ (top) and 0.2 (bottom). Filled and open squares are calculations from Eqs. (23) and (26). Filled and open circles correspond to Eqs. (29) and (30).

curves are well fitted by Eq. (23), and the nonlinear ones are reasonably well described by Eq.(29). Also included in Fig. 4 are the curves for \mathcal{F} computed using the same values of κH . For strongly charged coatings $\mathcal{F} \approx \Delta\psi$, confirming predictions of Eq.(30). When $\rho = 0$, \mathcal{F} is finite and its value is given by (26). This equation also predicts a parabolic growth of \mathcal{F} at small ρ , which is well seen in Fig. 4.

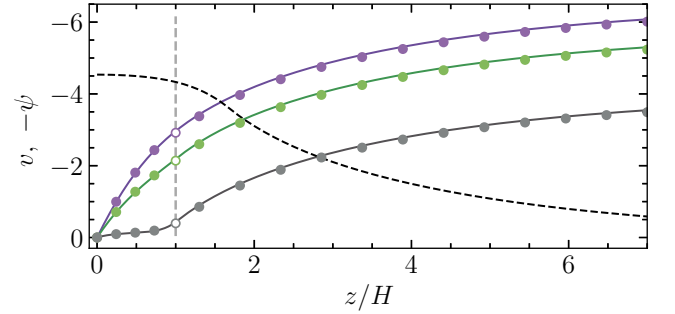


FIG. 5. The profiles v computed using $\kappa H = 0.3$ and $\rho = 50$ with $\mathcal{K}H = 0.1, 1$, and 5 (solid curves from top to bottom). Dashed line shows the electrostatic potential profile taken with the negative sign, $-\psi$. Filled circles show predictions of Eqs.(13) and (14). Open circles correspond to v_s calculated from Eq. (15).

We now turn to the electro-osmotic velocity. The velocity profiles computed using three $\mathcal{K}H$ in the range from 0.1 (small) to 5 (relatively large) are shown in Fig. 5. They have been obtained using $\kappa H = 0.3$ and $\rho = 50$. Note that with these parameters $\kappa H \sqrt{\rho} \approx 2.1$, $\rho\kappa H = 15$, and $\rho(\kappa H)^2 = 4.5$, so in our terms we deal with a non-thick highly charged film of moderate value of $\rho(\kappa H)^2$. Also included is the computed ψ -profile for this film. As described in Sec. II, the electrostatic potential of a non-thick film is generally nonuniform throughout the system. Its maximum value (at the wall) reaches about 4.5 , indicating that nonlinear electrostatic effects become significant.

The theoretical curves calculated from Eq.(13) for v_o using v_s defined by Eq.(15) and from Eq.(14) for v_i coincide with the numerical data. It can be seen that on reducing \mathcal{KH} the value of $-v_o$ increases. All outer velocity profiles are of the same shape that is set by ψ_o , indicating that the dramatic increase in $-v_o$ upon decreasing \mathcal{KH} is induced by changes in v_s only. At very large z/H the curves for v_o saturate to $v_\infty = -\zeta$ (not shown).

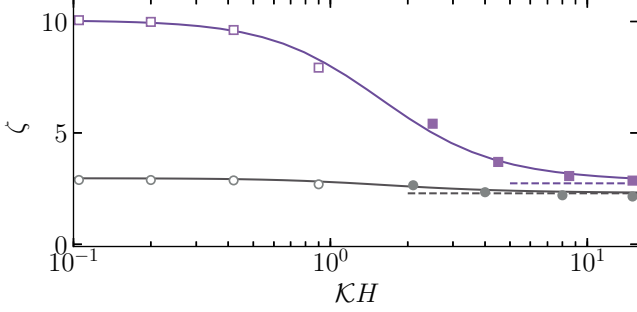


FIG. 6. Zeta potential as a function of \mathcal{KH} computed for $\kappa H = 0.8$ and 0.2 (solid curves from top to bottom) and $\rho = 20$. Dashed lines show ψ_s . Open and filled circles show predictions of Eqs.(35) and (36). Open and filled squares are obtained using Eqs.(39) and (40).

Fig. 6 intends to indicate the range of ζ that is encountered at different \mathcal{KH} . For this numerical example we use films of $\kappa H = 0.2$ and 0.8 , the same as in Fig. 4, and explore the case of $\rho = 20$. With these parameters $\rho(\kappa H)^2 = 0.8$ and 12.8 . These values differ significantly and correspond to different limits (or quasi-thin and quasi-thick films) described in Sec. III B, but the surface potentials, which are also shown in Fig. 6, are quite close (and not small). In the chosen range of values of \mathcal{KH} , which are neither too small nor quite large, zeta potentials of both films reduce strictly monotonically. We see that the value of ζ is much larger for the quasi-thick film of $\kappa H = 0.8$, where ζ can exceed ψ_s in several times. For a quasi-thin film of $\kappa H = 0.2$ the zeta potential is higher than ψ_s , but not much. The parts of the ζ -curves corresponding to $\mathcal{KH} \leq 1$ are well described by Eqs.(35) and (39), pointing out that this asymptotic approximations have validity well beyond the range of the original assumptions (see Sec. III). When $\mathcal{KH} \geq 2$, the decay of ζ is well consistent with predictions of Eqs.(36) and (40), indicating that the latter are also valid well outside the range of their formal applicability. As is usual, $\zeta \rightarrow \psi_s$ as $\mathcal{KH} \rightarrow \infty$.

We now fix $\kappa H = 0.5$ and compute ζ as a function of ρ using $\mathcal{KH} = 0.6$ and 3 . The results are plotted in Fig. 7, and compared with upper and lower bounds on ζ given by Eqs.(3) and (4). The computed at finite \mathcal{KH} zeta potentials are naturally confined between these two values. For small $\rho(\kappa H)^2$ we observe a rapid increase of ζ with ρ that is well described by Eqs. (34) and (36). As ρ is increased, $\rho(\kappa H)^2$ is shifted to a large value and

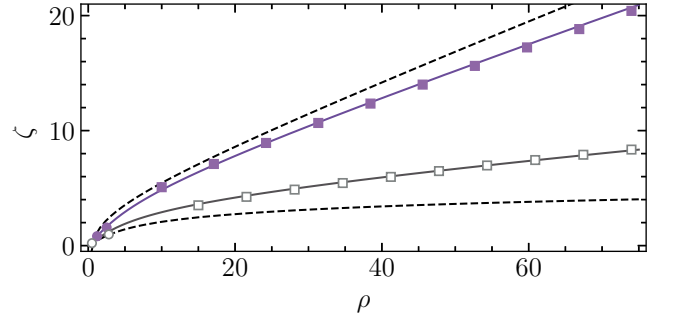


FIG. 7. Zeta-potential ζ computed for a film of $\kappa H = 0.7$ as a function of ρ for fixed $\mathcal{KH} = 0.6$ and 3 (upper and lower solid curves). Filled and open circles show calculations from Eqs.(34) and (36). Filled and open squares are obtained using Eqs.(39) and (40). Dashed curves indicate upper and lower bounds on ζ .

formulas (39) and (40) become very accurate.

V. TOWARDS SWITCHING SURFACE AND ZETA POTENTIALS BY SALT

So far we have considered ψ_s , ψ_o , and ζ using dimensionless variables, such as ρ , κH , \mathcal{KH} , and their combinations. Additional insight into the problem can be gleaned by expressing ζ as a function of characteristic length scales. These are the geometric length H , the hydrodynamic one Λ , and, of course, the electrostatic length λ_D . We recall that a useful formula for 1:1 electrolyte is [36]

$$\lambda_D[\text{nm}] = \frac{0.305[\text{nm}]}{\sqrt{c_\infty[\text{mol/L}]}} \quad (41)$$

and the dependence of ψ_s and ζ on λ_D in the equations below reflects their dependence on c_∞ . The latter is often probed in electrokinetic experiments, where a decrease of both potentials with salt is observed [33, 43, 44]. We stress, however, that the measurements have been often conducted by using only a very narrow range of relatively large c_∞ since existing linear theories could not provide a reasonable interpretation of data at low concentrations, where potentials are high.

It is also convenient to introduce a new electrostatic length of the problem

$$\ell = \sqrt{\frac{e}{4\pi\ell_B\varrho}} \propto \varrho^{-1/2}, \quad (42)$$

which is inversely proportional to the square root of the volume charge density, but does not depend on the bulk salt concentration.

The definition of dimensionless ρ can then be reformulated as

$$\rho = \left(\frac{\lambda_D}{\ell}\right)^2 \quad (43)$$

This suggests that it is the ratio of two electrostatic length scales of the problem that determines whether coatings are weakly or strongly charged. It is clear that an interesting “cross-over” behavior must occur for some intermediate values c_∞ that corresponds to $\lambda_D \simeq \ell$. We return to this important point below.

Condition (7) of a non-thick film then becomes

$$\frac{H}{\lambda_D} \left(1 + \left(\frac{\lambda_D}{\ell} \right)^4 \right)^{1/4} \gg 1, \quad (44)$$

i.e. $H/\lambda_D \gg 1$ for weakly charged films, and $H/\ell \gg 1$ for highly charged films. It is instructive to mention that an electrostatic thickness of highly charged films is equal to H/ℓ and does not depend on salt. Therefore, such films are thin when $H/\ell \ll 1$, but weakly charged films are thin when $H/\lambda_D \ll 1$.

The combinations of dimensionless parameters that control ψ_s , ψ_0 , and ζ can then be related to ℓ as

$$\rho \kappa H = \frac{\lambda_D H}{\ell^2}, \quad \rho (\kappa H)^2 = \left(\frac{H}{\ell} \right)^2, \quad \rho \left(\frac{\kappa}{\mathcal{K}} \right)^2 = \left(\frac{\Lambda}{\ell} \right)^2 \quad (45)$$

Eqs.(45) illustrate that there exist several length scales, lying always in the nanometric range, which determine different regimes of the electro-osmotic flow. Another important conclusion from Eqs.(45) is that $\rho (\kappa H)^2$ and $\rho (\kappa/\mathcal{K})^2$ do not depend on the salt concentration in the bulk. Accordingly, the dependence on salt is hidden only in $\rho \kappa H$, which is the function of λ_D .

We now present some results illustrating the role of length scales and showing that for films of a given H/ℓ the electrostatic regimes (of thin and thick films, or highly and weakly charged coatings) can be tuned by the concentration of salt. Let us now keep fixed $H = 15$ nm and consider two films, of $\ell = 5$ and 30 nm, which gives $H/\ell = 3$ and 0.5. These values of ℓ corresponds to $\rho = 360$ and 10 kC/m³, and we note that our larger value of ρ is close to the maximal one reported in experiments [45, 46]. In our concentration range λ_D/ℓ reduces from 60 down to 0.6 for the film of $\ell = 5$ nm, and from 10 down to 0.1 for that of $\ell = 30$ nm. It is easy to check that with the chosen parameters both model films fall to a category of non-thick.

We begin with the treatment of ψ_s obtained from the numerical solution of Eq.(5). Fig. 8 summarize different regimes in the $(H/\ell, H/\lambda_D)$ plane, where the magnitude of computed ψ_s is reflected by color. The smallest and largest values of H/ℓ in this diagram coincide with those of the two model films specified above, and the range of H/λ_D corresponds to c_∞ from 10^{-6} to 10^{-3} mol/L. It is now useful to divide the $(H/\ell, H/\lambda_D)$ plane into two regions, of weakly and strongly charged films, where the above scaling expressions for ψ_s approximately hold. We first remark that the conditions of weakly and highly charged coatings summarized in Table I coincide when $\rho = 1$. Consequently, we include in Fig. 8 (dotted) straight line that corresponds to $\lambda_D/\ell = 1$ (which is equivalent to $\rho = 1$) separating weakly and

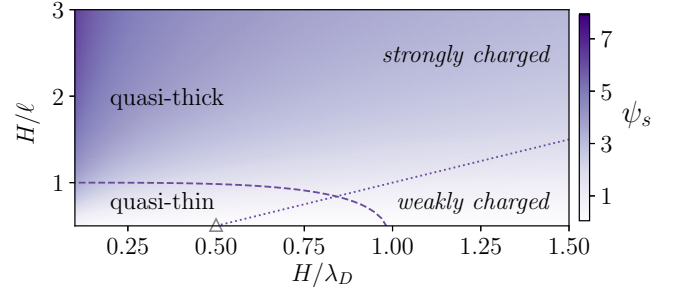


FIG. 8. Schematic representation of various electrostatic regimes for a non-thick porous film. The colorbar values of ψ_s ascend from top to bottom. The diagram is plotted in the $(H/\ell, H/\lambda_D)$ plane. Dotted line separates the regions, where coatings obey a linear theory, and where they can only be described using a non-linear theory. Dashed curve separates regions of quasi-thick and quasi-thin films as discussed in the text. Open triangle marks the point of $c_\infty = c_\infty^\Delta$.

highly charged surfaces. When H/ℓ is below this line a simple linear theory can be employed. However, for larger H/ℓ the Poisson-Boltzmann equation (5) cannot be linearized. Apart from this line, another crossover

locus, $\frac{H}{\lambda_D} \left(1 + \left(\frac{\lambda_D}{\ell} \right)^4 \right)^{1/4} = 1$ (separating the quasi-thin and quasi-thick film regions [47]) is shown by dashed curve. Of course, in reality at those two curves, the limiting solutions for ψ_s should crossover smoothly from one electrostatic regime to another. We can now conclude that in very dilute solutions both films are highly charged. However, at low salt the film of $\ell = 5$ nm is quasi-thick, but that of $\ell = 30$ nm is quasi-thin. If we increase H/λ_D (increase c_∞) for a film of $\ell = 30$, we move to a situation of weakly charged quasi-thin films. The intersection of the horizontal line $H/\ell = 0.5$ with the curve $\lambda_D/\ell = 1$ is marked with an open triangle and determines c_∞^Δ . On increasing H/λ_D further this film becomes weakly charged quasi-thick. The film of $\ell = 5$ nm is quasi-thick for all H/λ_D and becomes weakly charged at c_∞^Δ that is defined by the intersection of the line $H/\ell = 3$ with $\lambda_D/\ell = 1$.

The surface potential of a highly charged quasi-thick film can be obtained using Eq. (38)

$$\psi_s \simeq 2 \ln \left(\frac{\lambda_D}{\ell} \right) + \ln 2 - 1 \quad (46)$$

and depends only on λ_D/ℓ . However, when the highly-charged film is quasi-thin, ψ_s obeys Eq.(33) that can be rewritten as

$$\psi_s \simeq 2 \operatorname{arsinh} \left(\frac{\lambda_D H}{2 \ell^2} \right) - \left(\frac{H}{\ell} \right)^2 \quad (47)$$

Thus, in this situation ψ_s is defined by both λ_D/ℓ and H/ℓ .

At high salt, where both films become weakly charged and quasi-thick, to calculate ψ_s one can use (A7), which gives

$$\psi_s \simeq \frac{1}{2} \left(\frac{\lambda_D}{\ell} \right)^2 \propto \varrho c_\infty^{-1}, \quad (48)$$

i.e. the surface potential is again controlled solely by λ_D/ℓ .

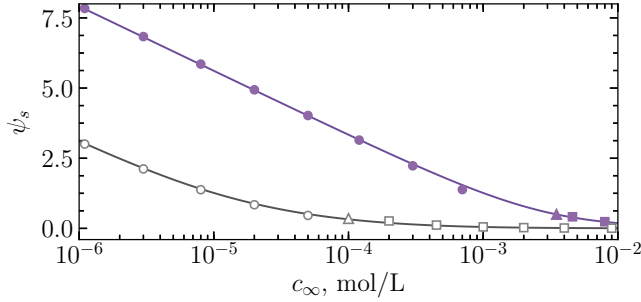


FIG. 9. ψ_s vs c_∞ computed using $H = 15$ nm and $\ell = 5$ (upper solid curve) and 30 nm (lower solid curve). Filled and open circles are obtained from Eqs.(46) and (47). Squares show predictions of Eq. (48), and triangles mark the points of the curves, where $\lambda_D = \ell$.

In Fig. 9 we plot ψ_s vs. c_∞ for these two specimen examples of the films. The surface potential is quite high at $c_\infty \simeq 10^{-6}$ mol/L (ca. 198 and 78 mV) and reduces with salt. At larger concentrations ψ_s becomes smaller than unity and practically vanishes when $c_\infty \geq 10^{-2}$ mol/L. To specify better the branches of low and high concentrations, in Fig. 9 we have marked c_∞^Δ and c_∞^\triangle by black and open triangles. For an upper curve computed using $\ell = 5$ nm this is located at $c_\infty^\Delta \simeq 3.7 \times 10^{-3}$ mol/L, and for a lower, of $\ell = 30$ nm, at $c_\infty^\triangle \simeq 10^{-4}$ mol/L. The corresponding surface potentials are $\psi_s \simeq 0.5$ and 0.3. Thus, when $\lambda_D/\ell = 1$, both films are of low surface potentials. The first film is quasi-thick as discussed above, and the branch of the curve with $c_\infty \geq c_\infty^\Delta$ is well fitted by Eq.(48). We recall that at c_∞^Δ the second film still remains quasi-thin and becomes quasi-thick, where (48) should be strictly valid, only when $c_\infty \simeq 4.3 \times 10^{-4}$ mol/L (see Fig. 8). We see, however, that the fit is quite good for $c_\infty \geq c_\infty^\Delta$, although at concentrations smaller than 4.3×10^{-4} mol/L there is some discrepancy, and Eq.(48) slightly overestimates ψ_s . Also included in Fig. 9 are theoretical calculations for low salt concentrations. We see that at c_∞ smaller than c_∞^Δ Eq.(46) is very accurate for a curve of $\ell = 5$ nm. When $\ell = 30$ nm, Eq.(47) provides an excellent fit to numerical data. Finally, we would like to stress that it is impossible to generate a very high ψ_s just by increasing ϱ . This is well seen in Fig. 9, where the upper curve corresponds to the film with 36 times larger ϱ than that for a film corresponding to a lower curve. The ratio of the values surface potentials for these two coatings is always smaller. Its largest value is equal to 18,

as follows from Eq.(48) for the high salt regime, where ψ_s is small. However, when ψ_s is large, its amplification with ϱ is very weak (only about 2 when $c_\infty \simeq 10^{-6}$ mol/L).

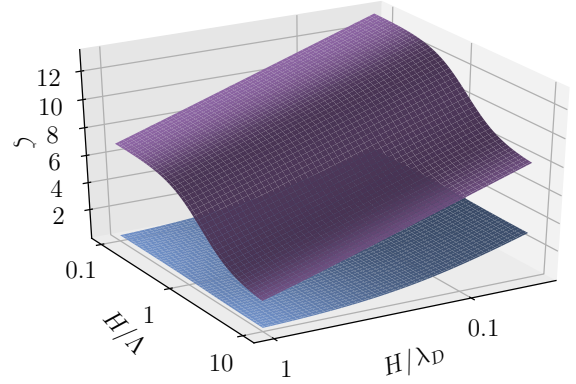


FIG. 10. ζ plotted as a function of two variables, H/λ_D and H/Λ , for a coating of thickness $H = 15$ nm using $\ell = 5$ (upper surface) and $\ell = 30$ nm (bottom surface). In the latter case $\zeta \simeq \psi_s$ as discussed in the text.

We are now on a position to calculate ζ , which generally depends on the Brinkman length Λ , and to contrast ζ to ψ_s . In Fig. 10 we plot ζ as a function of two variables, H/λ_D and H/Λ , for two porous coatings discussed above. We recall that they are of the same thickness, but their values of ℓ are different. An overall conclusion from this three dimensional plot is that for a film of $\ell = 5$ nm the zeta potential is larger and very sensitive to H/Λ . However, for a coating of $\ell = 30$ nm the effect of H/Λ on ζ , if any, is not discernible at the scale of Fig. 10. Indeed, as discussed in Sec. III B 1, in this case even at the infinite Brinkman length the zeta potential exceeds ψ_s , but very slightly (see also the lower curve in Fig. 6). Simple calculations show that $\zeta - \psi_s \leq (H/\ell)^2$, which is equal to 0.25, i.e. very small, when $\ell = 5$ nm. In other words, for this film $\zeta \simeq \psi_s$ and can be evaluated, depending on c_∞ that tunes an electrostatic regime, either using Eq.(47) or Eq.(48). Consequently, below we focus only on the quasi-thick film of $\ell = 5$ nm.

We now compute the salt dependence of ζ for a film of $\ell = 5$ nm by setting $\Lambda = 30$ and 3.75 nm. These give $H/\Lambda = 0.5$ and 4, which should correspond to large and small Brinkman length regimes (see Fig. 6). The results of numerical calculations are shown in Fig. 11 together with the computed bounds on ζ . We see that the difference between the upper and lower bounds is quite large. The numerical ζ -curves at finite Λ are confined between these bounds, and are of the same shape as ψ_s , but shifted towards higher values that grow with Λ until ζ reaches its upper attainable limit. When $c_\infty \leq c_\infty^\Delta$ the surface potential ψ_s is given by (46). At small H/Λ the expression for the zeta potential can be obtained from

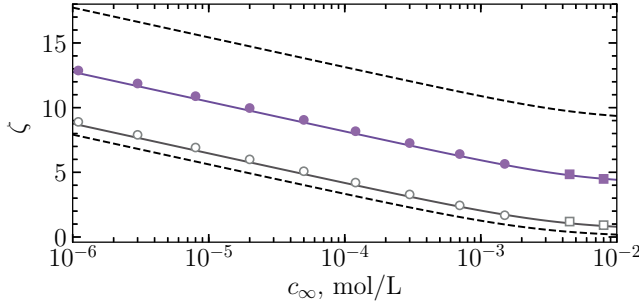


FIG. 11. ζ vs c_∞ computed using $\Lambda = 30$ nm (upper solid curve) and 3.75 nm (lower solid curve) for a film of $H = 15$ nm and $\ell = 5$ nm. Filled and open circles are obtained from Eqs. (49) and (50). Filled and open squares show calculations from Eqs.(51) and (52). Dashed curves show upper and lower bounds on ζ .

Eq. (39)

$$\zeta \simeq \psi_s + \frac{1}{2} \left(\frac{H}{\ell} \right)^2 \left[1 - \frac{5}{12} \left(\frac{H}{\Lambda} \right)^2 \right] + 1, \quad (49)$$

and when H/Λ is large, it follows from (40) that

$$\zeta \simeq \psi_s + \left(\frac{\Lambda}{\ell} \right)^2 + \frac{2\Lambda}{H} \quad (50)$$

In Sec. II we have clarified that the hydrodynamic permeability of the porous films $\propto H^2$ at low H/Λ and $\propto \Lambda^2$ when H/Λ is large. Thus, Eqs.(49) and (50) point strongly that the ratio of the hydrodynamic permeability to ℓ^2 is an important parameter controlling ζ . At larger concentrations, $c_\infty \geq c_\infty^\Delta$, small ψ_s is given by Eq.(48). Using then Eqs.(17) and (19) for small and large H/Λ we derive

$$\zeta \simeq \psi_s \left[2 - \frac{1}{4} \left(\frac{H}{\Lambda} \right)^2 \right] + \frac{1}{2} \left(\frac{H}{\ell} \right)^2 \left[1 - \frac{5}{12} \left(\frac{H}{\Lambda} \right)^2 \right], \quad (51)$$

$$\zeta \simeq \psi_s \left(1 + \frac{2\Lambda}{H} \right) + \left(\frac{\Lambda}{\ell} \right)^2 \quad (52)$$

We remark that again the ratio of the hydrodynamic permeability to ℓ^2 becomes an important factor that determines the amplification of ζ compared to ψ_s . The calculations from Eqs.(49)-(52) are also included in Fig. 9 and we see that provide an excellent fit to numerical data.

Thus, for quasi-thick films of a finite hydrodynamic permeability $\zeta \neq \psi_s$. As follows from Eqs.(49) - (52), besides ψ_s (that can be tuned by varying the concentration of salt) the value of ζ also reflects H/Λ and depends on the ratio of the hydrodynamic permeability to ℓ^2 .

VI. CONCLUDING REMARKS

We have presented a theory of surface and zeta potentials of non-thick porous coatings, i.e. those of a thick-

ness H comparable or smaller than that of the inner diffuse layer, of a finite hydrodynamic permeability. Our mean-field theory led to a number of asymptotic approximations, which are both simple and very accurate, and can easily be used to predict or to interpret ψ_s and ζ in different regimes, including situations when non-linear electrostatic effects become significant.

The main results of our work can be summarized as follows. We have introduced an electrostatic length scale $\ell \propto \varrho^{-1/2}$ and demonstrated that depending on its value two different scenarios occur. In the high salt concentration regimes, $\ell > \lambda_D \propto c_\infty^{-1/2}$, the non-thick porous films are weakly charged and their electrostatic properties can be described by linearized equations. These films effectively behave either as thin or thick depending on the values of H/λ_D and H/ℓ . We have also stressed the connection between the zeta potential and the Brinkman length, which is a characteristic of the hydrodynamic permeability of the porous film. Interestingly, the Brinkman length contribution to ζ permits to augment it compared to ψ_s only if $(H/\ell)^2$ is large, i.e. when films are quasi-thick.

Overall we conclude that tuning fluid transport inside a nanometric non-thick coating can dramatically affect the whole response of the large system to an applied electric field. Such a tuning can be achieved modifying its internal structure and charge density, or by varying film thickness, or concentration of an external salt solution.

ACKNOWLEDGMENTS

This work was supported by the Ministry of Science and Higher Education of the Russian Federation and by the German Research Foundation (grant 243/4-2) within the Priority Programme "Microswimmers - From Single Particle Motion to Collective Behaviour" (SPP 1726).

AUTHOR'S CONTRIBUTION

E.F.S. developed numerical codes, performed computations, and prepared the figures. N.B. participated in theoretical calculations. O.I.V. designed and supervised the project, developed the theory, and wrote the manuscript.

DATA AVAILABILITY STATEMENT

The data that support the findings of this study are available within the article.

Appendix A: The limit of low potentials

For completeness, in this Appendix we briefly discuss the case of low electrostatic potentials ($\psi \leq 1$), when Eq. (5) can be linearized to give

$$\psi''_{i,o} = \kappa^2 [\psi_{i,o} - \rho \Theta(H - z)] \quad (\text{A1})$$

Note that this case has been considered before by Ohshima and Ohki [14]. Here we present a compact derivation of expressions for ψ_0 and ψ_s in our (different) variables and complete the consideration by giving approximate expressions for $\Delta\psi$, \mathcal{F} . We also obtain an upper limit of ζ .

Integrating Eq. (A1) with prescribed boundary conditions (see Sec. II) one can easily obtain

$$\psi_i = \cosh(\kappa z) (\psi_0 - \rho) + \rho, \quad \psi_o = \psi_s e^{-\kappa(z-H)}, \quad (\text{A2})$$

which leads to

$$\psi_0 = \rho (1 - e^{-\kappa H}) \quad (\text{A3})$$

$$\psi_s = \rho \sinh(\kappa H) e^{-\kappa H} \quad (\text{A4})$$

It is then straightforward to obtain

$$\Delta\psi = \frac{\rho(1 - e^{-\kappa H})^2}{2}, \quad (\text{A5})$$

and

$$\mathcal{F} = 1 - e^{-\kappa H} \quad (\text{A6})$$

We recall that these equations are valid at any κH . At small κH they transform to Eq.(25), but at large κH they reduce to

$$\psi_0 \simeq \rho, \quad \psi_s \simeq \rho/2 \quad (\text{A7})$$

It is easy to verify that in fact the first equation of (A7) is valid already when $\kappa H \geq 5$, and the second when $\kappa H \geq 2$. In other words, they describes not only the thick films, but also valid for some non-thick ones that can be termed quasi-thick.

Interestingly, low potential films satisfying (A7) can potentially generate a high zeta-potential. Its upper achievable limit can be obtained using Eq.(3) and is given by

$$\zeta \simeq \rho + \frac{\rho(\kappa H)^2}{2}, \quad (\text{A8})$$

The last equation coincides with that for weakly charged thick films [15]. Dividing (A8) by (A4) we conclude that for low potential thick and quasi-thick films $\zeta/\psi_s \simeq 2 + (\kappa H)^2$.

-
- [1] M. von Smoluchowski, *Handbuch der Electricitat und des Magnetismus. Vol. 2*, edited by L. Graetz (Barth, J. A., Leipzig, 1921) pp. 366–428.
 - [2] O. I. Vinogradova, *Int. J. Miner. Proc.* **56**, 31 (1999).
 - [3] V. M. Muller, I. P. Sergeeva, V. D. Sobolev, and N. V. Churaev, *Colloid J. USSR* **48**, 606 (1986).
 - [4] L. Joly, C. Ybert, E. Trizac, and L. Bocquet, *Phys. Rev. Lett.* **93**, 257805 (2004).
 - [5] S. R. Maduar, A. V. Belyaev, V. Lobaskin, and O. I. Vinogradova, *Phys. Rev. Lett.* **114**, 118301 (2015).
 - [6] E. F. Silkina, E. S. Asmolov, and O. I. Vinogradova, *Phys. Chem. Chem. Phys.* **21**, 23036 (2019).
 - [7] O. I. Vinogradova and A. V. Belyaev, *J. Phys.: Condens. Matter* **23**, 184104 (2011).
 - [8] S. S. Bahga, O. I. Vinogradova, and M. Z. Bazant, *J. Fluid Mech.* **644**, 245 (2010).
 - [9] T. M. Squires, *Phys. Fluids* **20**, 092105 (2008).
 - [10] A. V. Belyaev and O. I. Vinogradova, *Phys. Rev. Lett.* **107**, 098301 (2011).
 - [11] G. S. Beavers and D. D. Joseph, *J. Fluid Mech.* **30**, 197 (1967).
 - [12] J. L. Anderson, *Annu. Rev. Fluid Mech.* **21**, 61 (1989).
 - [13] L. Bocquet and E. Charlaix, *Chem. Soc. Rev.* **39**, 1073 (2010).
 - [14] H. Ohshima and S. Ohki, *Biophys. J.* **47**, 673 (1985).
 - [15] O. I. Vinogradova, E. F. Silkina, N. Bag, and E. S. Asmolov, *Phys. Fluids* **32**, 102105 (2020).
 - [16] M. Cohen Stuart, W. T. S. Huck, J. Genzer, M. Muller, C. Ober, M. Stamm, G. B. Sukhorukov, I. Szleifer, V. V. Tsukruk, M. Urban, F. Winnik, S. Zauscher, I. Lizunov, and S. Minko, *Nature Mater* **9**, 101 (2010).
 - [17] B. Chollet, M. Li, E. Martwong, B. Bresson, C. Fretigny, P. Tabeling, and Y. Tran, *ACS Appl. Mater. Interfaces* **8**, 11729 (2016).
 - [18] M. Ballauff and O. Borisov, *Current Opinion Colloid Interface Science* **11**, 316 (2006).
 - [19] O. I. Vinogradova, O. V. Lebedeva, K. Vasilev, H. Gong, J. Garcia-Turiel, and B. S. Kim, *Biomacromolecules* **6**, 1495 (2005).
 - [20] S. Das, M. Banik, G. Chen, S. Sinha, and R. Mukherjee, *Soft Matter* **11**, 8550 (2015).
 - [21] A. van den Berg and M. Wessling, *Nature* **445**, 726 (2007).
 - [22] M. P. Pina, R. Mallada, M. Arruebo, M. Urbiztondo, N. Navascues, O. de la Iglesia, and J. Santamaria, *Microporous and Mesoporous Materials* **144**, 19 (2011).
 - [23] M. Lukatskaya, B. Dunn, and Y. Gogotsi, *Nat Commun* **7**, 12647 (2016).
 - [24] E. Donath and V. Pastushenko, *Bioelectrochem. Bioenergetics* **6**, 543 (1979).
 - [25] H. Ohshima and T. Kondo, *J. Colloid Interface Sci.* **135**, 443 (1990).
 - [26] H. Ohshima, *Adv. Colloid Interface Sci.* **62**, 189 (1995).
 - [27] E. F. Silkina, N. Bag, and O. I. Vinogradova, *Phys. Rev.*

- Fluids **5**, 123701 (2020).
- [28] J. F. L. Duval and H. P. van Leeuwen, *Langmuir* **20**, 10324 (2004).
- [29] J. F. L. Duval, *Langmuir* **21**, 3247 (2005).
- [30] H. Ohshima, *Theory of colloid and interfacial electric phenomena* (Elsevier, 2006).
- [31] A. C. Barbati and B. J. Kirby, *Soft Matter* **8**, 10598 (2012).
- [32] L. P. Yezek and H. P. van Leeuwen, *J. Colloid Interface Sci.* **278**, 243 (2004).
- [33] V. D. Sobolev, A. N. Filippov, T. A. Vorob'eva, and I. P. Sergeeva, *Colloid J.* **79**, 677 (2017).
- [34] G. Chen and S. Das, *J. Colloid Interface Sci.* **445**, 357 (2015).
- [35] D. Andelman, "Soft Condensed Matter Physics in Molecular and Cell Biology," (Taylor & Francis, New York, 2006) Chap. 6.
- [36] J. N. Israelachvili, *Intermolecular and Surface Forces*, 3rd ed. (Academic Press, 2011).
- [37] K. Z. Markov, in *Heterogeneous Media, Modelling and Simulation*, edited by K. Markov and L. Preziosi (Birkhauser Boston, 2000) Chap. 1, pp. 1–162.
- [38] S. Torquato, *Random Heterogeneous Materials: Microstructure and Macroscopic Properties* (Springer, 2002).
- [39] As a side note, since we consider here flat, infinite, and homogeneously charged porous layer, the electric field is the same everywhere (although the current density inside the porous layer is different from the outside) and normal flow is prohibited. In this case, one can neglect surface conduction (which tends to reduce electro-osmotic flow in finite size, curved, or heterogeneous systems) compared with bulk conduction ($Du = 0$), so we only discuss $v_{i,0}$.
- [40] A. V. Delgado, F. Gonzalez-Caballero, R. J. Hunter, L. K. Koopal, and J. Lyklema, *J. Colloid Interface Sci.* **309**, 194 (2007).
- [41] E. F. Silkina, T. Y. Molotilin, S. R. Maduar, and O. I. Vinogradova, *Soft Matter* **16**, 929 (2020).
- [42] G. Bader and U. Ascher, *SIAM J. Sci. and Stat. Comput.* **8**, 483 (1987).
- [43] M. Lorenzetti, E. Gongadze, M. Kulkarni, I. Junkar, and A. Iglič, *Nanoscale Res. Lett.* **11**, 378 (2016).
- [44] J. Irigoyen, V. B. Arekalyan, Z. Navoyan, J. Iturri, S. E. Moya, and E. Donath, *Soft Matter* **9**, 11609 (2013).
- [45] L. P. Yezek, J. F. M. Duval, and H. P. van Leeuwen, *Langmuir* **21**, 6220 (2005).
- [46] L. Braeken, B. Bettens, K. Boussu, P. Van der Meeren, J. Cocquyt, J. Vermant, and B. Van der Bruggen, *J. Membr. Sci.* **279**, 311 (2006).
- [47] This curve corresponds to a situation when the inner screening length is equal to H . So, formally it can also be seen as locus of a cross over between regimes of thick and thin films specified in Table I. However, since in our paper we focus only on the so-called non-thick films, we refer this curve to as a border between quasi-thin and quasi-thick coatings (see Sec.III B for detail), which is more appropriate in our context.